does not predict a streamwise stress level that is significantly higher than the simulation of Beaudan and Moin.[5] However, this can be explained by noting that, for this flow, most of the contribution to the Reynolds stress comes from fluctuations in a narrow frequency band extending from about $0.5\omega_{s_t}$ to $3.0\omega_{s_t}$, and in this frequency band, the energy in both simulations is comparable. Thus, even though the simulations of Beaudan and Moin[5] exhibit significant damping of the higher frequencies, this does not have a significant impact on the low-order turbulence statistics.

By comparing the vertical stress profiles at these locations, we observe that prediction from the two simulations at $x/D = 7.0$ is quite similar. At $x/D = 10.0$, the two simulations predict roughly the same peak stress level; however, the shape of the experimental profile matches the profile of Beaudan and Moin[5] better than it does for the current simulation. Furthermore, we have found that vertical velocity and shear stress profiles (not shown here) from both the simulations are also in reasonable agreement with experiments.[11]

Conclusions

It is found that in the downstream portion of the wake, where the grid is relatively coarse, the numerical dissipation inherent in the higher-order upwind-biased schemes removes substantial energy from roughly three-quarters of the resolved wave number range. In the central difference simulation, because there is no numerical dissipation, the smaller scales are more energetic. Because of this reduction in the damping of smaller scales, we find that the computed power spectra agree well with the experiment up to about half of the resolved wave number range. However, the enhanced energy in the small scales has no significant effect on the low-order statistics, and the mean velocity and Reynolds stress profiles in this region obtained from the two simulations are comparable. This is because most of the contribution to the normal stress comes from fluctuations whose frequency is centered in a narrow band around the shedding frequency and change in the energy of the small scales does not have a significant effect on the magnitudes of the Reynolds stresses. However, in applications such as flow generated noise and reactive flows, small-scale fluctuations play a crucial role, and it is, therefore, critical to retain the energy in the small scales. In such applications, energy conservative schemes would be preferable over upwind schemes. We also find that with about 20–30% smaller grid spacing, the second-order central difference scheme gives results that are comparable to those obtained by the high-order upwind biased schemes. The higher-order upwind based solver is more expensive on a per-point basis than the second-order central difference solver, and this partially offsets the additional cost of the increased resolution required by the second-order method. A drawback of the second-order central scheme is that the simulations are sensitive to numerical factors such as grid discontinuities and outflow boundary conditions and, thus, grids and boundary conditions have to be designed with extreme care.

Acknowledgments

This work was supported by the Office of Naval Research under Grant N00014-95-1-0221. We thank L. M. Lourenco and C. Shih for their private communication, "Characteristics of the Plane Turbulent Near Wake of a Circular Cylinder. A Particle Image Velocimetry Study." We would also like to thank Thomas Lund for his careful reading of the manuscript and helpful suggestions.

References

[1]Germano, M., Piomelli, U., Moin, P., and Cabot, W. A., "Dynamic Subgrid-Scale Eddy Viscosity Model," *Physics of Fluids A*, Vol. 3, No. 7, 1991, pp. 1760–1765.

[2]Ghosal, S., Lund, T. S., Moin, P., and Akselvoll, K., "A Dynamic Localization Model for Large-Eddy Simulation of Turbulent Flows," *Journal of Fluid Mechanics*, Vol. 286, March 1995, pp. 229–255.

[3]Piomelli, U., "High Reynolds Number Calculations Using the Dynamic Subgrid-Scale Stress Model," *Physics of Fluids A*, Vol. 5, No. 6, 1993, pp. 1484–1490.

[4]Rai, M. M., and Moin, P., "Direct Simulation of Turbulent Flows Using Finite-Difference Schemes," *Journal of Computational Physics*, Vol. 109, No. 2, 1991, pp. 169–192.

[5]Beaudan, P., and Moin, P., "Numerical Experiments on the Flow Past a Circular Cylinders at Sub-Critical Reynolds Numbers," Dept. of Mechanical Engineering, Rept. TF-62, Stanford Univ., Stanford, CA, Dec. 1994.

[6]Ong, L., and Wallace, J., "The Velocity Field of the Turbulent Very Near Wake of a Circular Cylinder," *Experiments in Fluids*, Vol. 20, No. 6, 1996, pp. 441–453.

[7]Akselvoll, K., and Moin, P., "Large-Eddy Simulation of Turbulent Confined Coannular Jets," *Journal of Fluid Mechanics*, Vol. 315, May 1994, pp. 387–411.

[8]Lund, T. S., and Moin, P., "Large-Eddy Simulation of a Concave Wall Boundary Layer," *International Journal of Heat and Fluid Flow*, Vol. 17, No. 3, 1996, pp. 290–295.

[9]Choi, H., Moin, P., and Kim, J., "Direct Numerical Simulation of Flow Over Riblets," *Journal of Fluid Mechanics*, Vol. 255, Oct. 1994, pp. 503–539.

[10]Lilly, D. K., "A Proposed Modification of the Germano Subgrid-Scale Closure Method," *Physics of Fluids A*, Vol. 4, No. 3, 1992, pp. 633–635.

[11]Mittal, R., "Progress in LES of Flow Past a Circular Cylinder," *CTR Annual Research Briefs*, Center for Turbulence Research, Stanford Univ., Stanford, CA, 1996, pp. 233–242.

[12]Press, W. H., Teukolsky, S. A., Vetterling, W. T., and Flannery, B. P., *Numerical Recipes in Fortran*, Cambridge Univ. Press, New York, 1992.

C. G. Speziale
Associate Editor

Three-Dimensional Finite Difference Method for Rotordynamic Fluid Forces on Seals

Morgan Williams,* Wei Chen,† Laura Brozowski,‡ and Anthony Eastland§
The Boeing Company, Canoga Park, California 91309-7922

Nomenclature

d	= amplitude of shaft whirl motion eccentricity
$\boldsymbol{E}$, $\boldsymbol{F}$, $\boldsymbol{G}$	= flux vectors in x, y, and z coordinate directions, respectively
F_n	= shaft normal force, $F_y y(t) + F_z z(t)$
F_t	= shaft tangential force, $F_y z(t) - F_z y(t)$
F_y, F_z	= shaft fluid pressure forces in y and z directions, respectively
k	= turbulence kinetic energy
p	= static pressure
$\boldsymbol{Q}$	= vector of flow variables
$\boldsymbol{S}$	= vector of momentum equation source terms
t	= time
$\boldsymbol{U}$	= vector of velocity variables
u, v, w	= Cartesian velocity components in the x, y, and z coordinate directions, respectively
x, y, z	= Cartesian coordinates
x_t, y_t, z_t	= mesh speed (partial differentiation of position with respect to time)

Presented as Paper 96-2738 at the AIAA/ASME/SAE/ASEE 32nd Joint Propulsion Conference, Lake Buena Vista, FL, July 1–3, 1996; received Dec. 16, 1996; revision received March 24, 1997; accepted for publication April 7, 1997.

*Engineering Specialist, Computational Fluid Dynamics, Rocketdyne Division, Boeing North American, Mail Stop IB39, 6633 Canoga Avenue, P.O. Box 7922. E-mail: morgan.williams@boeing.com.

†Senior Engineering Specialist, Rotating Machinery Analysis, Rocketdyne Division, Boeing North American, Mail Stop IB49, 6633 Canoga Avenue, P.O. Box 7922. E-mail: wei-chung.chen@boeing.com.

‡Project Engineer, Rotating Machinery and Valves Development, Rocketdyne Division, Boeing North American, Mail Stop IA34, 6633 Canoga Avenue, P.O. Box 7922.

§Project Manager, RAPID, Rocketdyne Division, Boeing North American, Mail Stop IA34, 6633 Canoga Avenue, P.O. Box 7922.

β = Helmholtz pressure equation psuedocompressibility factor
Δt = time step
δp = incremental pressure correction
$\partial_t, \partial_x, \partial_y, \partial_z$ = partial differentiation with respect to time, x, y, and z, respectively
ε = turbulence kinetic energy dissipation
Ω = shaft whirl frequency
Ω/ω = whirl ratio
ω = shaft spin frequency
$\{\}, \{\}^T$ = row, column vectors

Subscripts and Superscripts

M = maximum number of subiterations between time level n and $n+1$
m = subiteration level, $1 \leq m \leq M$
n = time level, where t is equal to $n\Delta t$
T = transpose
v = viscous terms

Introduction

IN turbomachinery components such as seals and pumps with shrouded impellers, the shaft motion can induce fluid friction and added mass forces on the shaft itself. These rotordynamic forces can lead to self-excited vibrations of the shaft.

Currently, there is only one basic type of computational methodology in use to calculate rotordynamic forces: quasisteady finite difference methods.[1,2] These finite difference methods are commonly classified as quasisteady because some type of reference frame coordinate transformation is used to render the eccentrically moving shaft to a centered, stationary shaft with respect to a moving reference frame. These methods have shown good agreement between computed results and experimental data for annular seals.

A more general rotordynamics computational methodology would be based on the solution of the three-dimensional unsteady Navier–Stokes equations with moving boundaries, e.g., whirling rotor shaft. Such a methodology, by definition, would be more computer intensive than quasisteady Navier–Stokes schemes, but it would also offer the potential for greater flexibility and the ability to analyze the fluid–structure interaction within complex geometries[3] in a coupled fashion.

The purpose of this Note is to present a time-accurate Navier–Stokes based method suitable for the calculation of rotordynamic coefficients for the incompressible flow regime. Results are presented for a long seal and a shrouded impeller.

Numerical Method

The current three-dimensional numerical rotordynamic algorithm is derived from the unsteady scheme described in Refs. 4 and 5.

Overview of Rotordynamic Fluid Force Calculation

The primary goal of the numerical methodology is to calculate the fluid reaction force vector time history and to decompose it into normal and tangential components.

The current overall Navier–Stokes procedure begins by obtaining a steady-state solution for the geometry of interest. The steady-state solution is then used as an initial condition for the unsteady calculations. The rotor shaft moves with an imposed harmonic motion, and the unsteady calculations are carried out until time periodicity is observed. The force time history is then processed to obtain the desired components.

Governing Flow Equations

The equations of motion for a three-dimensional, unsteady incompressible viscous fluid are

$$\nabla \cdot \boldsymbol{U} = 0 \tag{1a}$$

$$\partial_t \boldsymbol{Q} + \partial_x(\boldsymbol{E} - \boldsymbol{E}_v) + \partial_y(\boldsymbol{F} - \boldsymbol{F}_v) + \partial_z(\boldsymbol{G} - \boldsymbol{G}_v) = \boldsymbol{S} \tag{1b}$$

$$\{x(t), y(t), z(t)\}_{bc} = \{0, d \cdot \sin\Omega t, d \cdot \cos\Omega t\} \tag{1c}$$

where

$$\boldsymbol{Q} = \{u, v, w, k, \varepsilon\}^T$$

$$\boldsymbol{E} = \{u''u + p, u''v, u''w, u''k, u''\varepsilon\}^T$$

$$\boldsymbol{F} = \{v''u, v''v + p, v''w, v''k, v''\varepsilon\}^T$$

$$\boldsymbol{G} = \{w''u, w''v, w''w + p, w''k, w''\varepsilon\}^T$$

and $\boldsymbol{E}_v$, $\boldsymbol{F}_v$, and $\boldsymbol{G}_v$ are the standard viscous flux terms and are not modified for moving meshes; $\boldsymbol{S}$ includes the source terms for the standard k–ε turbulence model, and they require no modification for moving meshes. Here, x is in the axial direction and $\boldsymbol{U}$ is a vector composed of u, v, and w.

The effect of moving boundaries and mesh points on the governing flow equations are accounted for in the convective flux terms. The mesh speed components are (x_t, y_t, z_t); $u'' = (u - x_t)$, $v'' = (v - y_t)$, and $w'' = (w - z_t)$. Equation (1c) represents the imposed harmonic motion on the boundary of interest, e.g., rotor shaft.

The governing equations are assumed to be nondimensionalized with respect to a reference velocity Vref and length Lref. The reference time $t$ref is given as Lref/Vref. The reference pressure is given as $\rho V\text{ref}^2$; the density ρ is simply a constant.

Spatial Discretization

A second-order finite difference scheme with arbitrary node numbering is used to discretize the flow equations. The set of governing flow equations is formulated in terms of the standard nonorthogonal generalized coordinate system. Batina's[6] dynamic mesh movement algorithm is used to adjust the interior mesh nodes to the movement of the boundary nodes.

Time Integration

Euler (first-order) time-implicit discretization of the governing equations is used. Calculations are started from a valid initial state (e.g., $\boldsymbol{Q}^{n=0}$), and the unsteady flow is initiated by moving the rotor shaft to its new location at time $(n+1)\Delta t$ [Eq. (1c)]. Then the discretized momentum equation is solved:

$$(\boldsymbol{Q}^{n,m} - \boldsymbol{Q}^n)/\Delta t + \partial_x(\boldsymbol{E} - \boldsymbol{E}_v)^{n,m} + \partial_y(\boldsymbol{F} - \boldsymbol{F}_v)^{n,m} + \partial_z(\boldsymbol{G} - \boldsymbol{G}_v)^{n,m} = \boldsymbol{S}^{n,m-1} \tag{2}$$

where Δt is the numerical time step and the index n indicates the time level ($t = n\Delta t$); m is the subiteration or fractional step level, where $m = 1, 2, \ldots, M$; the counter M indicates the total number of subiterations, e.g., $\boldsymbol{Q}^{n+1} = \boldsymbol{Q}^{n,M}$. In the flux terms $\boldsymbol{E}^{n,m}$, $\boldsymbol{F}^{n,m}$, and $\boldsymbol{G}^{n,m}$, the pressure is evaluated at the previous subiteration level ($p^{n,m-1}$) and nonlinear terms are linearized about the $n, m-1$ level, e.g., $u^{n,m}u^{n,m} = u^{n,m-1}u^{n,m}$.

To help enforce the continuity equation, the Helmholtz pressure equation is solved:

$$\beta(\delta p) - \nabla \cdot \alpha\nabla(\delta p) = -\nabla \cdot \boldsymbol{U}^{n,m} \tag{3}$$

with the corrected velocity field given as

$$\boldsymbol{U}^{n,m+1} = \boldsymbol{U}^{n,m} - \alpha\nabla(\delta p) \tag{4}$$

and the next iterate for the pressure at interior mesh nodes is given by

$$p^{n,m+1} = p^{n,m} + \omega_p[(\delta p) - (\delta p)_{\text{ref}}] \tag{5}$$

where β is the Helmholtz pressure parameter,[4] ω_p is an underrelaxation factor, and $(\delta p)_{\text{ref}}$ is the calculated pressure correction at an arbitrary flow node; α is a 3×3 diagonal matrix that depends on the form of the iterative equation used to solve the momentum equation. The Helmholtz pressure equation is a key component of the three-dimensional rotordynamic algorithm: it allows the use of a time-implicit formulation without requiring a machine zero accurate solution of the pressure equation at each time subiteration. The discretized flow equations were solved by using successive overrelaxation (SOR). About 10 and 20 SOR iterations were used for the discretized momentum and Helmholtz pressure equations, respectively. Implicit Neumann boundary conditions were used for the pressure correction δp. This ensures consistency with the velocity divergence free condition at all time levels. Extrapolation boundary conditions were used to calculate $p^{n,m+1}$ at the boundaries.

Numerical Results

To demonstrate and assess the current rotordynamic fluid reaction force algorithm performance, calculations were performed for a whirling long seal and a whirling shrouded impeller. Flow meshes were generated algebraically. All of the cases were three dimensional because the whirling motion breaks the usual geometric axisymmetry. No systematic attempt was made to optimize the flow meshes or solution accuracy.

Long Seal

Kanemori and Iwatsubo[7] conducted an experimental study of a long seal to determine the dynamic fluid forces induced by the seal. They were able to measure the normal and tangential forces to within 12–15% of their respective magnitudes. The seal has an L/D of 3, a rotor radius of 39.656 mm, and a clearance of 0.394 mm. The working fluid is water, and the mass flow rate was 0.0762 kg/s (16 kPa δp). The seal inlet swirl ratio (inlet tangential velocity/shaft speed) was 0.4, the rotor spin frequency was 1080 rpm, and the whirl eccentricity was 0.049 mm. The baseline flow model consists of a 35 × 11 × 16 (axial × radial × azimuth) flow mesh. A grid refinement study with 11, 16, and 21 nodes in the azimuth direction was performed for $\Omega/\omega = \pm 0.4$ and with a numerical time step equal to 0.1. The calculated shaft forces varied by less than 7% between the baseline grid (16 azimuth nodes) and the fine grid (21 azimuth nodes).

Because the primary focus is unsteady phenomena, the numerical error was studied by examining the effect of Δt (numerical time step) on the calculated results. The effect of time truncation error on the calculated normal forces per unit whirl eccentricity amplitude (F_n/d) for $\Omega/\omega = \pm 0.4$ is shown in Fig. 1. Recall that the normal force is calculated from the time-dependent force history and, therefore, reflects the unsteady forces on the shaft. The smaller the Δt, the more accurate is the solution (it approaches the experimental value, which is, of course, independent of Δt), but more overall time steps are required to resolve a cycle of whirling. A numerical time step of 0.025 (non-dimensional) was used for all of the subsequent calculations.

Seven whirl cases were calculated. The calculated reaction forces per unit whirl amplitude are compared to the experimental data in Fig. 2. In general, the agreement is good.

Shrouded Impeller

Guinzburg[8] constructed an experimental apparatus to simulate the leakage flow along a conical shroud from the impeller discharge to the impeller inlet (Fig. 3) and the normal and tangential forces for various revolutions per minute and flow conditions were measured. The present authors could not find a discussion of measurement errors in Guinzburg's thesis. The working fluid was water. The particular case calculated here was for a mass flow rate of 1.892 liter/s and a rotor spin of 500 rpm. The seal rotor radius was 93.7 mm, and the clearance was 4.24 mm. The whirl eccentricity was 1.18 mm. A zero inlet swirl boundary condition was assumed for all of the computed flow cases. The computer time required for a typical case was approximately 117 SPARC 20 h for 150 time steps.

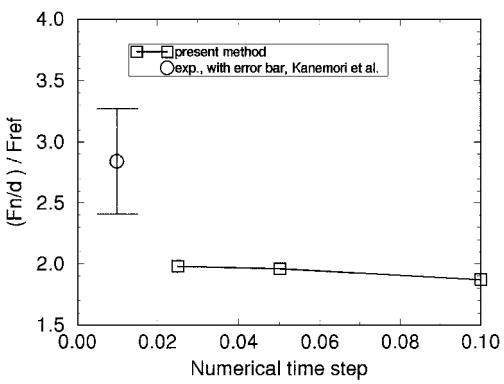

Fig. 1 Effect of numerical time step (truncation error) on the magnitude of the unsteady reaction forces per unit whirl eccentricity amplitude for a long seal with a whirling shaft ($\Omega/\omega = \pm 0.4$ and Fref = 0.324 MN/m); the experimental data point shown is, of course, independent of Δt but is included to show the level of agreement.

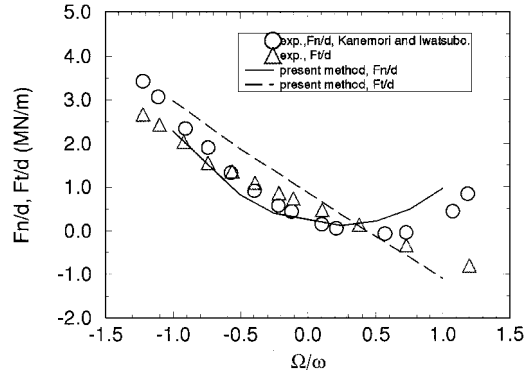

Fig. 2 Effect of whirl ratio (Ω/ω) on the fluid reaction forces per unit whirl eccentricity amplitude for a long seal.

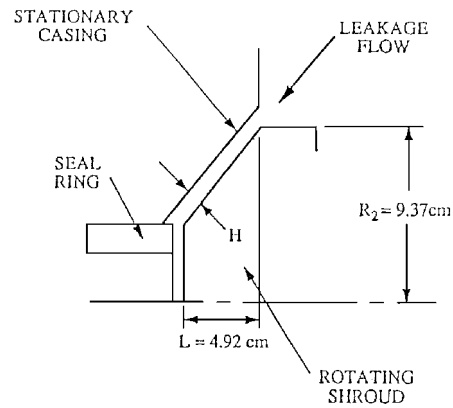

Fig. 3 Schematic of conical impeller shroud.[8]

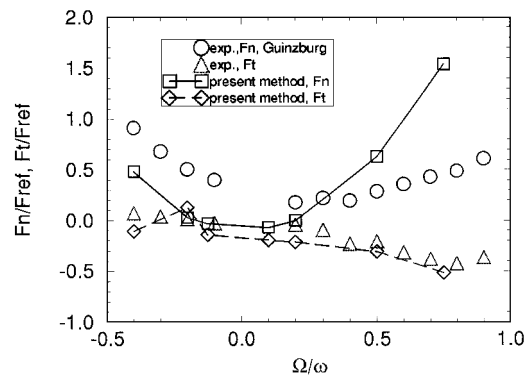

Fig. 4 Comparison of computed reaction forces with experiment for the whirling conical impeller shroud (Fref = 4.4 N).

The calculated normal and tangential forces F_n and F_t, respectively, are compared to the experimental data in Fig. 4 for this complicated flow case. The normal force prediction, in general, shows the correct trends. The predicted tangential force shows the correct trend and shows good agreement with the experimental values.

Numerical errors were examined by increasing the number subiterations to 600 from the baseline 200. The computed solution achieved time periodicity in fewer time steps but the overall calculated normal and tangential forces did not change significantly.

Conclusions

A moving boundary Navier–Stokes method suitable for three-dimensional incompressible rotordynamic fluid reaction force calculations was presented. The method incorporates the Helmholtz pressure method for unsteady incompressible flow. The rotordynamic methodology was used to calculate the motion-induced forces for several turbomachinery type components and it has the potential to be useful for practical applications, e.g., labyrinth seals and tapered seals. Future work should examine, more closely, the issue

of consistent boundary conditions for general three-dimensional rotordynamic configurations and time-discretization truncation error.

References

[1]Dietzen, F. J., and Nordmann, R., "Calculating Rotordynamic Coefficients of Seals by Finite-Difference Techniques," *Journal of Tribology*, Vol. 109, July 1987, pp. 388–394.

[2]Baskharone, E. A., and Hensel, S. J., "A Finite-Element Perturbation Approach to Fluid/Rotor Interaction in Turbomachinery Elements. Part 1: Theory," *Journal of Fluids Engineering*, Vol. 113, Sept. 1991, pp. 353–361.

[3]Chen, W. C., and Jackson, E. D., "A General Theory for Eccentric and Misalignment Effects in High-Pressure Annular Seals," *ASLE Transactions*, Vol. 30, No. 3, 1987, pp. 293–301.

[4]Williams, M., "A Helmholtz Pressure Equation Method for the Calculation of Unsteady Incompressible Viscous Flows," *International Journal of Numerical Methods in Fluids*, Vol. 14, No. 1, 1992, pp. 1–12.

[5]Williams, M., "A Spatially High-Order Unstructured Grid Based Computational Scheme for Incompressible Fluid-Structure Interaction," AIAA Paper 94-2832, June, 1994.

[6]Batina, J. T., "Unsteady Euler Airfoil Solutions Using Unstructured Dynamic Meshes," *AIAA Journal*, Vol. 28, No. 8, 1990, pp. 1381–1388.

[7]Kanemori, Y., and Iwatsubo, T., "Experimental Study of Dynamic Fluid Forces and Moments for a Long Annular Seal," *Journal of Tribology*, Vol. 114, No. 10, pp. 773–778.

[8]Guinzburg, A., "Rotordynamic Forces Generated by Discharge-to-suction Leakage Flows in Centrifugal Pumps," Ph.D. Thesis, Dept. of Engineering and Applied Science, California Inst. of Technology, Pasadena, CA, Jan. 1992.

P. R. Bandyopadhyay
Associate Editor

Boundary Integral Equations for Notch Problems in Plane Thermoelasticity

C. K. Chao*
National Taiwan Institute of Technology, Taipei 106, Taiwan, Republic of China

Introduction

THE magnification of stresses at geometric discontinuities is of great importance in engineering design. In particular, local stresses may be highly enhanced in notched materials arising from abrupt changes of shape. This would result in a substantial decrease of the load-bearing capacity of structural members. Various methods of calculating stress concentration factors have been developed for two-dimensional elasticity problems. Using a series expansion method, Ling[1] solved elastic problems with different types of notches. Bowie and Freese[2] analyzed the notch problem by using complex variable theory in conjunction with the conformal mapping method. Nisitani[3] used the method of body force (or Green's function) to solve the notch problem in a semi-infinite plate or in a strip.

An alternative method for solving notch problems may be formulated in terms of a system of boundary integral equations. This method has clear advantages in solving the problem by applying a numerical treatment. In the derivation of boundary integral equations, the selection of the auxiliary function determines whether the kernels have weak or strong singularities. The kernel with Cauchy-type singularity has been widely used to solve many crack problems.[4] On the other hand, the integral equation with a logarithmic kernel has been proved to easily perform the numerical computation by Cheung and Chen.[5] This method with weak singularity has been used to solve some crack problems associated with an elastic half-plane medium,[6] two bonded thermoelastic half-plane media,[7] and thermoelastic circular inclusion perfectly bonded in an infinite matrix.[8] Based on the earlier derivation, Chen and Cheung[9] recently reformulated a new boundary integral equation to deal with the notch problem in plane elasticity. In this Note, we aim to further extend the aforementioned method to solve notch problems in plane thermoelasticity. In the derivation of singular integral equations, instead of using the components of heat flux and the components of stress, the resultant heat flow $\boldsymbol{Q}$ and the resultant force $-Y + iX$ are used to formulate the boundary conditions along the notch surface. This would result in singular integral equations with a logarithmic kernel instead of a Cauchy-type kernel. Three different types of notches in an infinite medium under a remote uniform heat flow are considered as our examples to illustrate the use of the approach. Some available exact solutions are provided to compare with the calculated numerical results to demonstrate the accuracy of the study.

Received May 25, 1996; revision received Feb. 3, 1997; accepted for publication March 24, 1997.

*Professor, Department of Mechanical Engineering.

Formulation of Integral Equation: Thermal Field

For the two-dimensional steady-state heat conduction problem, the temperature function, which satisfies the Laplace equation, can be expressed in terms of a single analytic function $\theta(\boldsymbol{z})$. With this function, both the temperature T and the resultant heat flow $\boldsymbol{Q}$ are written as

$$T = \mathrm{Re}[\theta(\boldsymbol{z})] \tag{1}$$

$$\boldsymbol{Q} = \int (\boldsymbol{q}_x \, \mathrm{d}y - \boldsymbol{q}_y \, \mathrm{d}x) = -k \, \mathrm{Im}[\theta(\boldsymbol{z})] \tag{2}$$

where Re and Im denote the real and imaginary parts of the bracketed expression, respectively. The quantities $\boldsymbol{q}_x$ and $\boldsymbol{q}_y$ in Eq. (2) are the components of heat flux in the x and y directions, respectively, and k is the heat conductivity. Consider a remote uniform heat flux approached from the negative x axis obstructed by the presence of an insulated notch or hole in an infinite medium. The current problem can be treated as a sum of the corresponding infinite medium problem without notches and a corrective term. The solution associated with the former problem can be easily expressed as

$$\boldsymbol{Q}_0(\boldsymbol{z}) = \boldsymbol{q} \, \mathrm{Im}[\boldsymbol{z}] \tag{3}$$

with $\boldsymbol{q}$ being the strength of heat flux applied at infinity.

On the other hand, a corrective solution associated with an infinite medium with a single notch can be obtained by assuming a continuous distribution of dislocations with the density $b_0(s)$ placed along a given contour L as

$$\theta(\boldsymbol{z}) = -\frac{i}{2\pi} \int_L \log(\boldsymbol{z} - t) b_0(s) \, \mathrm{d}s \tag{4}$$

The resultant heat flow across the notch surface can be obtained by substituting Eq. (4) into Eq. (2) as

$$\boldsymbol{Q}(\boldsymbol{z}) = \frac{k}{4\pi} \int_L [\log(\boldsymbol{z} - t) + \log(\bar{\boldsymbol{z}} - \bar{t})] \, \mathrm{d}s + c_0, \qquad \boldsymbol{z} \in L \tag{5}$$

where a bar will be used to indicate a conjugate complex quantity and c_0 is a constant to be determined.

Based on the superposition principle, the boundary integral equation for an infinite medium containing an insulated notch is then established as follows:

$$\frac{k}{2\pi} \int_L \log(|\boldsymbol{z} - t|) b_0(s) \, \mathrm{d}s + c_0 = -\boldsymbol{q} \, \mathrm{Im}[\boldsymbol{z}], \qquad \boldsymbol{z} \in L \tag{6}$$

In addition, the single-valued condition of the temperature must be satisfied, i.e.,

$$\int_L b_0(s) \, \mathrm{d}s = \boldsymbol{0} \tag{7}$$

Equation (6) together with Eq. (7) constitutes a boundary integral equation for solving the unknown function $b_0(s)$. Once the function $b_0(s)$ is determined, the temperature function $\theta(\boldsymbol{z})$ in Eq. (4) will be obtained accordingly.